

Generalized compactness limit from an arbitrary viewing angle

Tatsuya Matsumoto,^{1,2,3★} Ehud Nakar,⁴ and Tsvi Piran¹

¹*Racah Institute of Physics, Hebrew University, Jerusalem, 91904, Israel*

²*Department of Physics, Graduate School of Science, Kyoto University, Kyoto 606-8502, Japan*

³*JSPS Research Fellow*

⁴*The Raymond and Beverly Sackler School of Physics and Astronomy, Tel Aviv University, Tel Aviv 69978, Israel*

17 March 2022

ABSTRACT

A γ -ray source must have a limited optical depth to pair production. This simple condition, called compactness, implies that gamma-ray bursts (GRBs) must involve a highly relativistic motion ($\Gamma \gtrsim 100$) giving the first and most important clue on their nature. So far, this condition has been discussed under the assumption that the γ -ray sources are viewed on-axis, that is, by an observer within the beaming cone of the relativistic source. Recently, following the detection of the weak short GRB 170817A, an extensive interest arose in the possibility that some γ -ray sources are viewed off-axis. We generalize here the compactness formalism for an arbitrary viewing angle taking several possible opacity processes and γ -ray spectra into account. We find that for a given observables (peak luminosity, temporal variability, and spectra) the minimal Lorentz factor, Γ_{\min} , is obtained, as expected, for an on-axis observer. More remarkably we find that compactness dictates also a maximal viewing angle, $\theta_{\max} \simeq 1/2\Gamma_{\min}$. Our limit implies for regular GRBs a very small allowed viewing angle ($\lesssim 10^{-2}$ rad), making it extremely unlikely that they are viewed off-axis. For GRB 170817A we confirm earlier results that rule out the possibility that the observed γ -rays were seen by an on-axis observer as a regular short GRB. The short GRB 150101B was also suggested to be an off-axis event. We show that its maximal viewing angle $\lesssim 0.05$ rad, which is inconsistent with the off-axis model. Finally we show that for low luminosity GRBs, compactness does not exclude by itself an off-axis model, but when combined with other consideration this option is strongly disfavored.

1 INTRODUCTION

The first and most important clue on the nature of gamma-ray bursts (GRBs) arose from the compactness argument. The combination of huge luminosity, rapid variability, and a non-thermal spectrum implied that GRBs must involve a relativistic motion. A Newtonian calculation that uses the size implied by the temporal variability and the observed spectrum yields a huge optical depth ($\sim 10^{13}$) for pair production ($\gamma\gamma \rightarrow e^+e^-$). Such a source would have had no photons above the electron’s rest mass energy, $m_e c^2$, where m_e and c is the electron mass and the speed of light, respectively, and a thermal spectrum below it. This is the so-called compactness problem (Ruderman 1975; Schmidt 1978). It was used as an argument in favor of the Galactic origin (as such bursts are of course much less energetic) or even for “new physics”. Compactness problem is resolved, for bright cosmological GRB sources, by introducing a relativistic motion towards us (Ruderman 1975; Paczynski 1986; Goodman 1986; Krolik & Pier 1991, see also Woltjer 1966 in the context of compactness in active galactic nuclei). The observed photon energy is boosted and the observed timescale gets shorter. Both effects reduce the optical depth. For typical

GRBs, the relativistic optical depth is $\sim 10^{13}/\Gamma^6$, where Γ is the Lorentz factor, and one needs $\Gamma \gtrsim 10^2$ to obtain the observed gamma-ray signal (Piran 1997, 1999; Lithwick & Sari 2001). This was the first and still strongest indication that GRBs involve a ultra-relativistic motion, as commonly understood today.

So far, the compactness problem has been discussed only for sources observed on-axis. Here, we define “on- (off-) axis” view when an observer sees the source from the inside (outside) the relativistic beaming cone whose angular width is $\simeq 1/\Gamma$. Clearly, off-axis observers see a γ -ray transient with a lower luminosity, lower typical photon energies and longer variability timescale than those observed by an on-axis one and therefore their compactness limits on the source are different.

There have been numerous suggestions that dimmer and softer transients, for example low-luminosity GRBs (ℓ GRBs), are regular GRBs observed off-axis (e.g., Nakamura 1998; Eichler & Levinson 1999; Woosley et al. 1999; Ioka & Nakamura 2001; Yamazaki et al. 2003; Waxman 2004). Similar suggestions (Goldstein et al. 2017; Murguía-Berthier et al. 2017; Ioka & Nakamura 2018) were made shortly following the detection of the very weak short GRB

(sGRB) 170817A (Abbott et al. 2017b; Goldstein et al. 2017; Savchenko et al. 2017). However, these suggestions did not take into account the compactness problem (Kasliwal et al. 2017). In an earlier paper (Matsumoto et al. 2019), we have shown that compactness when combined with other conditions imposed by the afterglow observations (Mooley et al. 2018) rules out the possibility that the observed γ -rays in sGRB 170817A arose from a regular sGRB jet viewed off-axis (cf. Eichler 2017). We concluded that another γ -ray emission mechanism is needed, e.g. shock breakout of a cocoon (Kasliwal et al. 2017; Nakar et al. 2018; Lazzati et al. 2018; Kathirgamaraju et al. 2018; Gottlieb et al. 2018; Bromberg et al. 2018; Pozanenko et al. 2018; Beloborodov et al. 2018).

Motivated by this example, we derive here the general compactness condition for an arbitrary γ -ray source for a general viewing angle. Our work generalizes Lithwick & Sari (2001) that derived general compactness conditions for an on-axis observer. In addition to the common condition that requires that the photons with the highest energy can escape from the source without pair production, we consider other processes that can dominate the γ -ray opacity: the Compton opacity of pairs produced by annihilation of the high energy photons and the Compton opacity of the electrons in the outflow. At times, e.g. for sGRB 170817A, those latter conditions are more important than the first one that is more commonly considered. To do that we derive the optical depth to the different opacity sources as a function of the Lorentz factor and the viewing angle for the source.

We organize this paper as follows: In §2.1 we review the processes that determines the γ -rays opacity at a source. Next, we derive in §2.2 an expression of the optical depth for given observables (peak luminosity, temporal variability, and spectra) as well as the source Lorentz factor and viewing angle. Using this expression we obtain, in §2.3, limits on the Lorentz factor of the source and on its viewing angle. We apply the general argument in §3 to typical GRBs, to the low-luminosity sGRBs 170817A and 150101B, and to several low-luminosity long GRBs (*ll*GRBs). We summarize our results in §4.

2 COMPACTNESS

2.1 Opacity sources of γ -rays

We begin by recapitulating the essence of the three processes that determines the opacity at the source. The first two arise from pairs produced via two-photon pair production of the high energy photons. As such they depend on the observed spectrum. The third source of opacity arises from the electrons that exist within the source. While it does not depend on the spectrum its significance depends on whether the outflow is baryonic or not. Following Lithwick & Sari (2001), we denote these cases as limits A, B, and C.

In the following we relate the observables in the observer frame, denoted by Q to those at the source rest frame, denoted by Q' . The source is moving with a Lorentz factor Γ ($\beta \equiv \sqrt{1 - 1/\Gamma^2}$) and the radiation field is roughly isotropic in the source local frame. The energy of the photons, ϵ , as

seen in the different frames is related via the Doppler factor:

$$\delta_D(\theta, \Gamma) \equiv \frac{1}{\Gamma(1 - \beta \cos \theta)}, \quad (1)$$

such that

$$\epsilon = \delta_D(\theta, \Gamma) \epsilon'. \quad (2)$$

The angle θ is measured from the center of the gamma-ray emitting region (see below and Fig. 1).¹ We ignore redshift effects that can be trivially added later (see §2.3).

2.1.1 Limit A : Pair production

The most common limit, denoted following Lithwick & Sari (2001) limit A, arises by demanding that the highest energy photon observed with energy ϵ_{\max} escapes from the source without annihilating with other photons. A naive interpretation is simply $\epsilon_{\max}/\delta_D(\theta, \Gamma) \leq m_e c^2$. However this assumes that the spectrum has an unrealistic sharp cut-off at ϵ_{\max} (e.g., in typical GRBs the number of photons above ϵ_{\max} should drop by ~ 10 orders of magnitude before the source becomes optically thin to ϵ_{\max} photons under this assumption). There is no reason to assume such a coincidence since ϵ_{\max} depends on the detector. Either the flux above ϵ_{\max} is too low to be detected or it is just the upper limit of the detector's window. A priori it is not reasonable to assume that the spectrum breaks just at this energy. It is most natural to extrapolate the observed spectrum to higher energies. The assumption that the spectrum can be extrapolated upwards is reasonable in the case that the upper part of the spectrum is a power-law and can be considered as conservative when considering an exponential cutoff. Note that by extrapolating one assumes only that photons more energetic than ϵ_{\max} are present at the source, not that they escape from it (namely the source does not have to be optically thin to photons with $\epsilon > \epsilon_{\max}$). To estimate the optical depth for pair production of a photon with ϵ_{\max} we define $\epsilon_{\text{th},A}(\epsilon_{\max})$ the minimal energy of the photons with which an ϵ_{\max} photon can annihilate:

$$\epsilon_{\text{th},A}(\epsilon_{\max}) = \frac{[\delta_D(\theta, \Gamma) m_e c^2]^2}{\epsilon_{\max}}; \text{ limit A.} \quad (3)$$

We then calculate the fraction, f , of photons above $\epsilon_{\text{th},A}$ and demand that their optical depth is sufficiently small. Limit A has been commonly used in the GRB literatures but, depending in particular on the spectral shape, it is not always the most stringent one.

2.1.2 Limit B : Scattering by pairs

For limit B, we consider the opacity attributable to the pairs created by self-annihilating photons. The energy threshold of photons which can self-annihilate is given by

$$\epsilon_{\text{th},B} = \delta_D(\theta, \Gamma) m_e c^2; \text{ limit B.} \quad (4)$$

¹ This definition of θ is different from the definition used by Matsumoto et al. (2019), where $\Delta\theta_{\text{obs}}$ is measured from the edge of the γ -ray emission region and not from its center.

We approximate the number of pairs as the number of photons with energy larger than the threshold energy, and calculate the fraction f , of photons above this threshold for a given observed spectrum.

Limit B is less known than limit A. However, at times it is more important. It dominates for bursts with a small maximal observed photon energy ϵ_{\max} , which is in particular the case when the bursts are dim or when the upper end of the observed spectrum is exponential (as in the case of a Comptonized power-law) rather than a power-law. Note that also here, like in limit A, the limit is dictated by an extrapolation of the observed spectrum to energies above the highest observed photon energy, and when a Comptonized spectrum is considered then this extrapolation is the most natural one.

2.1.3 Limit C : Electron scattering

A third source of opacity is optical depth of the source's electrons that accompany the baryons in the outflow. The total electron number can be estimated, from the baryon number, which in turn is determined by the energy budget. For any baryonic outflow, the thermal energy in the rest frame is larger than the total rest frame emitted photon energy. The thermal energy per baryon is given by $w - m_p c^2$, where w and m_p are the enthalpy per baryon and the proton mass, respectively. An extreme assumption for a baryonic outflow is that it was accelerated to its Lorentz factor Γ from rest and crossed a shock just before the emission took place. In that case $w \approx \Gamma m_p c^2$. Note that [Lithwick & Sari \(2001\)](#) assume here that the available baryonic energy is $w - m_p c^2 \approx m_p c^2$. Our estimate is larger by a factor of $\Gamma - 1$ and our limit is, correspondingly, less restrictive. The energetics argument limits the total baryon number as

$$\Gamma m_p c^2 N'_{\text{baryon}} \gtrsim \epsilon'_p N'_\gamma, \quad (5)$$

where ϵ'_p and N'_γ are the observed peak photon energy (peak energy of the energy flux) and the total photon number in the emitting region, respectively, such that the right-hand-side is approximately the total rest frame radiation energy. Clearly this estimation is valid only in the case that the energy source is the energy carried by the baryons (e.g. for an internal-shock model but not a Poynting flux dominated outflow).

For normal GRBs, limit C gives the weakest limit, hence not much attention was paid to it in terms of limit on the Lorentz factor. Instead it was used to put a lower limit on the emission radius. In this limit, pair production has nothing to do with the opacity, and the optical depth depends only on total observed radiation energy and it is independent of the specific observed spectrum.

2.2 The optical depth

We consider a general γ -ray transient, characterized by the following observables: (a) an isotropic γ -ray luminosity $L_{\gamma, \text{iso}}$, (b) a variable timescale (duration of an observed single pulse) δt , and (c) the photon spectrum $dN/d\epsilon$ with a peak energy ϵ_p (see Table 1). Using these observables, we evaluate the optical depth of the γ -ray transient taking the different limits into account. Note that in this section we

do not take redshift effects into account. However those are inserted later when we estimate the final results shown in Table 2.

The optical depth of γ -rays in the rest frame is given by (e.g., [Nakar 2007](#))

$$\tau \approx \frac{\sigma N'_s l'}{\pi \theta_\gamma^2 R^2 \Delta R'}. \quad (6)$$

σ is the relevant cross section, l' is the path length of the photons within the region before escaping to the observer, and N'_s is the number of annihilating photons in limit A, number of produced pairs in limit B, and number of source electrons in limit C. θ_γ , R , and $\Delta R'$ are the characteristic angle of the γ -ray emitting region, radial distance where the emission episode takes place, and the thickness of the γ -ray emitting region, respectively. The angle and distance are measured in the lab frame.

The cross section for pair production peaks slightly above the threshold (given by Eq. 3) and then it decreases quickly with energy. For a power-law photon spectrum with a photon index -2 , the average value of the cross section becomes $(11/180)\sigma_T$ where σ_T is the Thomson cross section, ([Svensson 1987](#); [Lithwick & Sari 2001](#)). We use this factor for a power-law spectrum (PL). We don't use it for a cut-off power-law spectrum that declines sharply at high energy. In the following, we still use the notation σ_T for simplicity, but restore the coefficient in the summarizing Table 2.

Generally, the outflow that produces the γ -ray emission has an angular structure, e.g., luminosity and Lorentz factor distributions that depend on the angle. Each point on the outflow contributes to the observed γ -ray flux with different intensity and Doppler boost. In [Matsumoto et al. \(2019\)](#), we showed that, because of the sensitive dependence of the Doppler boost on the viewing angle, unless there is an extreme fine tuning a small patch of the outflow dominates the observed γ -rays. Thus, we can reasonably assume that the luminosity and Lorentz factor over the patch are approximately constant. We denote this region as the γ -ray emitting region and approximate the geometry of the emitting source by a characteristic angular size θ_γ over which the luminosity and the Lorentz factor do not vary significantly. It is viewed from an angle θ , measured from the center of this region (see Fig. 1).

For a small viewing angle and a large Lorentz factor, the angular variation of the Doppler factor depends on the product $\Gamma\theta$. Hence, for $\theta < 1/\Gamma$, the observer is on-axis and relativistic beaming dictates the size of the γ -ray emitting region: $\theta_\gamma \leq 1/\Gamma$. For $\theta > 1/\Gamma$, the observer is off-axis and the observed γ -ray emission is suppressed by the Doppler de-beaming. Hence, only a region of size θ can contribute significantly. Overall, the size of the γ -ray emitting region satisfies:

$$\theta_\gamma \leq \max\left\{\frac{1}{\Gamma}, \theta\right\}. \quad (7)$$

We turn now to evaluate the various quantities that determine the optical depth (Eq. 6) using the observables. For limits A and B, we write N'_s as

$$N'_s = f N'_\gamma. \quad (8)$$

Here, f is the fraction of photons whose energy is larger than the thresholds $\epsilon_{\text{th,A}}$ (Eq. 3) or $\epsilon_{\text{th,B}}$ (Eq. 4). N'_γ is the total

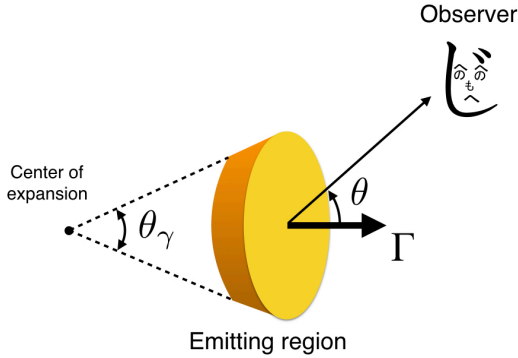


Figure 1. Schematic picture of a γ -ray emitting region and an observer. Over this region, the luminosity and Lorentz factor are uniform.

number of photons:

$$N'_\gamma \simeq \frac{4\pi d^2 S_\gamma}{\delta_D^2(\theta, \Gamma) \epsilon_p} \simeq \frac{L_{\gamma, \text{iso}} \delta t}{\delta_D^2(\theta, \Gamma) \epsilon_p}, \quad (9)$$

where d is distance to the burst, $S_\gamma \simeq L_{\gamma, \text{iso}} \delta t / 4\pi d^2$ is observed γ -ray fluence during δt and $L_{\gamma, \text{iso}}$ the isotropic equivalent luminosity. In deriving this relation, we have used the transformation of the solid angles $\Delta\Omega = \Delta\Omega' / \delta_D^2(\theta, \Gamma)$, and assumed that the source radiates photons isotropically in the rest frame.

For a normalized photon spectrum, the photon fraction, f , is calculated as

$$f = \int_{\epsilon_{\text{th}}}^{\infty} \frac{dN}{d\epsilon} d\epsilon, \quad (10)$$

where $\epsilon_{\text{th}} = \epsilon_{\text{th,A}}$ or $\epsilon_{\text{th,B}}$ and we assume that the observed high end of the photon spectrum extends to higher energies. We consider two spectra: a power-law in the relevant (high energy) segment (denoted PL) and a power-law with an exponential cut-off, also called a Comptonized spectrum (CPL):

$$\frac{dN}{d\epsilon} \propto \begin{cases} \epsilon^{\beta_p} & ; \text{PL}, \\ \epsilon^{\alpha_p} \exp\left[-\frac{\epsilon(\alpha_p + 2)}{\epsilon_p}\right] & ; \text{CPL}, \end{cases} \quad (11a)$$

where (following here the standard notation in the GRB literature) β_p and α_p are the spectral indices for the high energy part of the Band function in the PL case and the power-law of the CPL case, respectively. The fraction of annihilating photons is given by:

$$f \sim \begin{cases} \left(\frac{\epsilon_{\text{th}}}{\epsilon_p}\right)^{\beta_p + 1} & ; \text{PL}, \\ \left(\frac{\epsilon_{\text{th}}(\alpha_p + 2)}{\epsilon_p}\right)^{\alpha_p} \exp\left(-\frac{\epsilon_{\text{th}}(\alpha_p + 2)}{\epsilon_p}\right) & ; \text{CPL}. \end{cases} \quad (12a)$$

In the PL case, we consider only the high energy part of the

spectrum and we normalize the spectrum at the peak energy ϵ_p .²

In limit C, electrons associated with baryons in the out-flow scatter the photons. The total baryon number is given by Eq. (5) :

$$N'_s = N'_{\text{baryon}} \gtrsim \frac{\epsilon_p}{\Gamma \delta_D(\theta, \Gamma) m_p c^2} N'_\gamma. \quad (13)$$

Since this value is also proportional to N'_γ , we can use the same form of N'_s as in limits A and B by defining the fraction, f , as

$$f \equiv \frac{\epsilon_p}{\Gamma \delta_D(\theta, \Gamma) m_p c^2}; \text{ limit C}. \quad (14)$$

The crux of the argument in the off-axis case is to estimate, using the observed variability time scale δt , the emission radius, R , and use it to obtain a limit on the optical depth τ . The observed pulse duration is the sum of three times. The angular spreading time

$$\delta t_{\text{ang}} = \frac{2R}{c} \begin{cases} \sin(\theta) \sin\left(\frac{\theta_\gamma}{2}\right) & ; \theta > \frac{\theta_\gamma}{2}, \\ 1 - \cos\left[\frac{1}{2}\left(\theta + \frac{\theta_\gamma}{2}\right)\right] & ; \theta < \frac{\theta_\gamma}{2}, \end{cases} \quad (15)$$

the radial timescale

$$\delta t_{\text{radial}} \equiv \frac{dR}{c\beta} \left[1 - \beta \cos \theta\right] = \frac{dR}{c\beta \Gamma \delta_D(\theta, \Gamma)}, \quad (16)$$

where $dR \leq R$ is the distance crossed by the source while it was active, and the light crossing time δt_{lc} of the photon shell. Clearly $\delta t \simeq \max\{\delta t_{\text{ang}}, \delta t_{\text{radial}}, \delta t_{\text{lc}}\}$.

In Appendix A, we show that if $\delta t_{\text{lc}} > (\delta t_{\text{radial}}, \delta t_{\text{ang}})$, i.e. the light crossing time is the longest, then the limits on the opacity are more constraining than those obtained in case that it is not. Therefore, we consider conservatively $\delta t_{\text{lc}} < \delta t_{\text{radial}}$, in which case $l' \simeq \Delta R'$ as a photon emitted from one side of the emitting region towards the observer crosses the entire emitting region by the time that the radius doubles (this point is also shown in appendix A). Taking $l' \simeq \Delta R'$, Eq. (6) becomes:

$$\tau \simeq \frac{\sigma N'_s}{\pi \theta_\gamma^2 R^2}. \quad (17)$$

Next we examine the limits on τ when R is constrained by the condition $\delta t = \max\{\delta t_{\text{ang}}, \delta t_{\text{radial}}\}$. We show in appendix B that in the off-axis case the limit obtained under the assumption that $\delta t = \delta t_{\text{ang}}$, is similar to the one obtained in case that $\delta t = \delta t_{\text{rad}}$ and $dR = R$. We also show that this is also the case for an on-axis observer, unless there is an anomalously narrow source with $\theta_\gamma \ll 1/\Gamma$. We therefore continue deriving the limit on τ by by setting $\delta t = \delta t_{\text{rad}}$ where $dR = R$, but we stress that the limit we obtain is applicable for any type of source when observed off-axis, including a point source that radiates instantaneously in time, and to any source with $\theta_\gamma \sim 1/\Gamma$ when observed on-axis.

Substituting Eqs. (8), (9), and (16) with $dR = R$ into Eq. (17) we find that θ_γ appears in the denominator and hence θ_γ has to attain its maximal value, $\theta_\gamma = \max\{1/\Gamma, \theta\}$,

² Strictly speaking, for the Band function (Band et al. 1993), the peak energy should be replaced with $\epsilon_p/(\alpha_p, \text{Band} + 2)$ where α_p, Band is the low energy power-law index of the Band function.

to minimize τ . Overall we obtain a lower limit on the optical depth:

$$\begin{aligned}\tau \geq \tau_{\min} &= \left\{ \frac{\sigma_{\Gamma}}{\pi c^2} \frac{L_{\gamma, \text{iso}}}{\epsilon_p \delta t} \right\} \left[\frac{f}{[\max\{1/\Gamma, \theta\}]^2 \beta \Gamma^2 \delta_{\text{D}}^4(\theta, \Gamma)} \right] \\ &= \mathcal{L} \left[\frac{f}{[\max\{1/\Gamma, \theta\}]^2 \beta \Gamma^2 \delta_{\text{D}}^4(\theta, \Gamma)} \right],\end{aligned}\quad (18)$$

where we define the dimensionless observable

$$\begin{aligned}\mathcal{L} &\equiv \frac{\sigma_{\Gamma}}{\pi c^2} \frac{L_{\gamma, \text{iso}}}{\epsilon_p \delta t} \\ &\simeq 1.5 \times 10^{13} \left(\frac{L_{\gamma, \text{iso}}}{10^{51} \text{ ergs/s}} \right) \left(\frac{\epsilon_p}{100 \text{ keV}} \right)^{-1} \left(\frac{\delta t}{0.1 \text{ s}} \right)^{-1}.\end{aligned}\quad (19)$$

Note that \mathcal{L} should be multiplied by the factor 11/180 for limit A and a PL spectrum (see Table 2).

Eq. (18) together with an estimate of f (obtained using Eq. 12a or 12b with energy thresholds Eq. 3 or 4 for limits A and B, and Eq. 14 for limit C) is a general form of the minimal optical depth for an observer from an arbitrary viewing angle. We stress that this is only a lower limit on the opacity obtained under optimal conditions that minimize the opacity. The actual conditions could be more stringent leading to a stronger limits on the Lorentz factor and on the viewing angle. Eq. (18) generalizes the common expression for the optical depth for an observer at $\theta = 0$ obtained by Lithwick & Sari (2001). As we see later this $\theta = 0$ expression is a very good approximation for all on-axis observers.

Table 2 summarizes the different possible forms that the expression (Eq. 18) takes for the various cases discussed here. We mark in colors the cases that correspond to typical GRBs and *ll*GRBs which are the subclass of long GRBs with low luminosity (see §3.4, for more detailed properties of *ll*GRBs).

2.3 Limits on Γ and θ

The fact that we observe bright γ -rays implies that the optical depth of the source is limited. The reasons for this limit depend on the spectrum. If the spectrum is highly non-thermal, as in the case of a high-energy power-law, then $\tau \lesssim 1$ since $\tau \gg 1$ leads to either a blackbody or a Wien spectrum. This argument is not applicable to a Comptonized spectrum since it can be a result of a sum of blackbody or Wein spectra with different temperatures (the sum is needed to produce a shallow power-law at low energies $\alpha_p < 3$). However, regardless of the spectral effects, $\tau > 1$ implies that the photons are trapped inside the source by scattering unless the source thickness is $\Delta R < R/(2\Gamma^2\tau^2)$. Therefore, $\tau \gg 1$ leads to an unrealistically thin source, so also in case of a Comptonized spectrum the optical depth cannot be too large. In the limits that we derive below we set $\tau_{\min} = 1$. If one is interested in the limit in case of a different value for τ_{\min} then the value of \mathcal{L} in Table 2 should be replaced by \mathcal{L}/τ_{\min} . Given the weak dependence of the various limits on the value of \mathcal{L} , the effect on the result for any reasonable value of τ_{\min} is minor.

Taking $\tau_{\min} = 1$, we obtain first a lower limit on the Lorentz factor for a given viewing angle. Examination of Eq. (18) reveals a product of \mathcal{L} that depends only on observational quantities and a term in square brackets that depends

on observables via f and on Γ and θ . In the following we isolate the part that depends on the observed quantities in f and we obtain an expression that depends just on Γ and θ that we solve for each set of observables.

This solution results in both a lower limit on Γ and an upper limit of θ . This is a result of the functional shape of the Doppler factor, which for $\Gamma \gg 1$ and $\theta \ll 1$ takes the form

$$\delta_{\text{D}}(\theta, \Gamma) \simeq \frac{2\Gamma}{1 + (\Gamma\theta)^2} \propto \begin{cases} \Gamma & ; \theta \lesssim \Gamma^{-1}, \\ \Gamma^{-1}\theta^{-2} & ; \theta \gtrsim \Gamma^{-1}. \end{cases}\quad (20)$$

For a given observing angle θ , the Doppler factor has a maximum at $\Gamma = 1/\theta$. It increases (decreases) with Γ for on-axis (off-axis) observers. Thus, for a given δ_{D} and a given observing angle θ there are either two solutions for Γ (an “on-axis” solution with $\theta < 1/\Gamma$ and an “off-axis” solution with $\theta > 1/\Gamma$) or no solution if the observing angle is too large.

This implies that compactness sets an upper limit on θ , consider the dependence of the minimal optical depth, τ_{\min} , on Γ

$$\tau_{\min} \propto \frac{f}{\theta_{\gamma}^2 \Gamma^2 \delta_{\text{D}}^4(\theta, \Gamma)} \propto \begin{cases} f\Gamma^{-4} & ; \theta \lesssim \Gamma^{-1}, \\ f\Gamma^2\theta^6 & ; \theta \gtrsim \Gamma^{-1}, \end{cases}\quad (21)$$

where $\theta_{\gamma} = \max\{1/\Gamma, \theta\}$. The photon fraction, f , is a decreasing function of δ_{D} (see Eqs. 3, 4, 12a, 12b, and 14) and hence for a fixed θ it is minimal at $\Gamma \simeq 1/\theta$. Therefore, for any value of θ the optical depth τ_{\min} obtains a minimal value for $\Gamma \simeq 1/\theta$. If this value is larger than unity then there is no solution for this value of θ . Now, setting $\Gamma = 1/\theta$ shows that τ_{\min} increases monotonically with θ . Therefore there is a maximal value of θ above which τ_{\min} must be larger than unity and the compactness limit cannot be satisfied. The behavior of τ_{\min} (Eq. 21) is easily understood as follows. Observation of a given flux implies a photon and particle density in the source that is a rapidly increasing function of θ (because larger θ moves the observer out of the beam), and that above some value of θ the implied source density implies $\tau > 1$, forbidden by compactness.

This can be seen in Fig. 2 which depicts the allowed regions, for two sets of parameters (see Table 2) resembling the observation of GRBs 170817A (left) and 090510 (right). The colored regions are values of Γ and θ where τ can be smaller than unity and the thick lines mark the solution for $\tau_{\min} = 1$. The allowed region is divided into on- and off-axis regions, where the minimal allowed Lorentz factor, Γ_{\min} is obtained for an on-axis observer. At $\theta = 0$ we recover the results of Lithwick & Sari (2001). Fig. 2 shows that for each model and each set of parameters there is a maximal value of θ above which there is no solution. Thus, while the compactness argument was brought up originally to put on a lower limit on the Lorentz factor, it turns out that at the same time it provides a corresponding limit on the maximal viewing angle θ_{\max} . This maximal angle is obtained for an observer located on the boundary between the “on-axis” and “off-axis” configurations, namely, for $\theta \simeq 1/\Gamma$ and as we see later $\theta \simeq 1/2\Gamma_{\min}$.

The compactness limits on Γ and θ can be solved numerically for any set of parameters, however, it is illustrative to derive an analytic approximation. We therefore estimate the allowed regions of the different limits (A, B, and C) for a given set of parameters by approximating $\beta = 1$ and

Table 1. Summary of observables.

Symbol	Observables Definition	Typical values used in Fig. 2	
		left	right
$L_{\gamma, \text{iso}}$	Isotropic γ -ray luminosity	$10^{47} \text{ erg s}^{-1}$	$10^{53} \text{ erg s}^{-1}$
δt	Variable timescale	0.1 s	0.01 s
ϵ_p	Peak energy of photons	0.5 MeV	4 MeV
ϵ_{max}	Maximum energy of photons	0.5 MeV	30 GeV
β_p	Spectral index (PL)	-2	-2
α_p	Spectral index (CPL)	-1	-1
z	redshift	0	1

Table 2. Summary of lower limits on the Doppler factor δ_D , the minimal Lorentz factor Γ_{min} , and the maximal viewing angle θ_{max} . The colored cells mark the relevant limits for typical GRBs (yellow) and ℓ GRBs (pink, see §3.4 for the properties of ℓ GRBs).

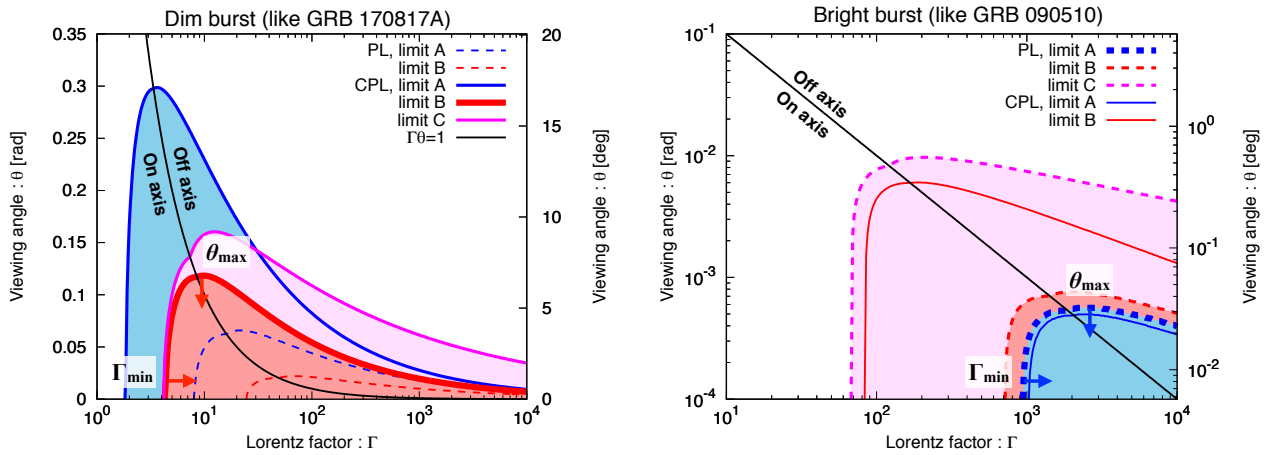
Spectrum	Limit	\mathcal{L}	\mathcal{E}	τ_{min}	$\delta_{D, \text{min}}$	Γ_{min}	θ_{max}
PL	limit A	$\frac{(11/180)\sigma_T}{\pi c^2} \frac{L_{\gamma, \text{iso}}}{\epsilon_p \delta t}$	$\frac{\epsilon_p \epsilon_{\text{max}} (1+z)^2}{(m_e c^2)^2}$	$\frac{\mathcal{L}}{\mathcal{E}^{\beta_p+1}} \delta_D^{2(\beta_p-1)}$	$(\frac{\mathcal{E}^{\beta_p+1}}{\mathcal{L}})^{\frac{1}{2(\beta_p-1)}}$	$\frac{1}{2} (\frac{\mathcal{E}^{\beta_p+1}}{\mathcal{L}})^{\frac{1}{2(\beta_p-1)}}$	$\frac{1}{2} (\frac{\mathcal{E}^{\beta_p+1}}{\mathcal{L}})^{\frac{1}{2(1-\beta_p)}}$
	limit B	$\frac{\sigma_T}{\pi c^2} \frac{L_{\gamma, \text{iso}}}{\epsilon_p \delta t}$	$\frac{\epsilon_p (1+z)}{m_e c^2}$	$\frac{\mathcal{L}}{\mathcal{E}^{\beta_p+1}} \delta_D^{\beta_p-3}$	$(\frac{\mathcal{E}^{\beta_p+1}}{\mathcal{L}})^{\frac{1}{\beta_p-3}}$	$\frac{1}{2} (\frac{\mathcal{E}^{\beta_p+1}}{\mathcal{L}})^{\frac{1}{\beta_p-3}}$	$\frac{1}{2} (\frac{\mathcal{E}^{\beta_p+1}}{\mathcal{L}})^{\frac{1}{3-\beta_p}}$
	limit C		$\frac{\epsilon_p (1+z)}{m_p c^2}$	$\frac{\mathcal{L} \mathcal{E}}{\Gamma \delta_D^5}$	-	$(\frac{\mathcal{L} \mathcal{E}}{32})^{1/6}$	$(2 \mathcal{L} \mathcal{E})^{-1/6}$
CPL	limit A		$\frac{\epsilon_p \epsilon_{\text{max}} (1+z)^2}{(m_e c^2)^2 (\alpha_p+2)}$	$\frac{\mathcal{L}}{\mathcal{E}^{\alpha_p}} \delta_D^{2(\alpha_p-2)} \exp(-\frac{\delta_D^2}{\mathcal{E}})$	Eq. (23)*	$\frac{\delta_{D, \text{min}}}{2}$	$\frac{1}{2\delta_{D, \text{min}}}$
	limit B	$\frac{\sigma_T}{\pi c^2} \frac{L_{\gamma, \text{iso}}}{\epsilon_p \delta t}$	$\frac{\epsilon_p (1+z)}{m_e c^2 (\alpha_p+2)}$	$\frac{\mathcal{L}}{\mathcal{E}^{\alpha_p}} \delta_D^{\alpha_p-4} \exp(-\frac{\delta_D}{\mathcal{E}})$	Eq. (23)*	$\frac{\delta_{D, \text{min}}}{2}$	$\frac{1}{2\delta_{D, \text{min}}}$
	limit C		$\frac{\epsilon_p (1+z)}{m_p c^2}$	$\frac{\mathcal{L} \mathcal{E}}{\Gamma \delta_D^5}$	-	$(\frac{\mathcal{L} \mathcal{E}}{32})^{1/6}$	$(2 \mathcal{L} \mathcal{E})^{-1/6}$

Limit A: ϵ_{max} photon can escape from the source without pair production.

Limit B: the emitting region is optically thin to Thomson scattering by pairs created by the γ -ray photons.

Limit C: the emitting region is optically thin to scattering by electrons in the source. The limit is relevant for a baryonic outflow and independent of the spectral shape.

* There is no analytic solution.

**Figure 2.** The allowed Lorentz factor and viewing angle imposed by compactness for two types of GRBs (see Table 1 for the specific parameters). The dashed and solid curves show the limits for PL and CPL spectra, respectively, and the different colored curves denote different limits (see also Table 2). Colored regions show the allowed regions for the relevant spectral shape CPL (left) and PL (right) spectra. The other spectral limit is also shown for a comparison. The black curves ($\Gamma\theta = 1$) divide the phase space to on and off-axis regions. Limit C is independent of the spectral shape. **Left:** Parameters corresponding to the dim and soft sGRB 170817 A. Limit B (red curves) gives the most restrictive constraint. **Right:** Parameters corresponding to the bright and hard sGRB 090510. Limit A (blue curves) gives the most severe limit. In particular the viewing angle is constrained to be a very small value, $\theta \lesssim 10^{-3}$ rad (Note that the viewing angle is shown in a logarithmic scale in this figure).

$\theta_\gamma = 1/\Gamma$ even for $\theta > 1/\Gamma$, which does not change the result significantly. With these approximations, the factor in square brackets in Eq. (18) depends only on the Doppler factor for limits A and B. We have an additional factor of Γ for limit C. The optical depth is characterized by three dimensionless parameters: \mathcal{L} (defined in Eq. (19)), \mathcal{E} , and the spectral index α_p or β_p . The dimensionless factor \mathcal{E} is defined as:

$$\mathcal{E} \equiv \begin{cases} \frac{\epsilon_p \epsilon_{\max}(1+z)^2}{(m_e c^2)^2} & ; \text{PL \& limit A,} \\ \frac{\epsilon_p(1+z)}{m_e c^2} & ; \text{PL \& limit B,} \\ \frac{\epsilon_p \epsilon_{\max}(1+z)^2}{(m_e c^2)^2(\alpha_p+2)} & ; \text{CPL \& limit A,} \\ \frac{\epsilon_p(1+z)}{m_e c^2(\alpha_p+2)} & ; \text{CPL \& limit B,} \\ \frac{\epsilon_p(1+z)}{m_p c^2} & ; \text{limit C.} \end{cases} \quad (22)$$

We have added here the redshift (z) dependence to the definition of \mathcal{E} . \mathcal{L} is independent of the redshift. There are three redshift effects (Lithwick & Sari 2001): (i) the distance d in Eq. (9) should be replaced by the luminosity distance $d \rightarrow d_L/(1+z)$. (ii) the timescales in Eq. (18) should be modified to $\delta t \rightarrow \delta t/(1+z)$ to account for the cosmological time dilation. As pointed out by Lithwick & Sari (2001), these two effects (i) and (ii) cancel out. (iii) the photon energy is also redshifted: $\epsilon \rightarrow \epsilon(1+z)$. This last effect modifies the threshold energy in Eqs. (3) and (4), and Eq. (14). Therefore, as noted above, the redshift changes only the parameter \mathcal{E} .

With these definitions, the minimal optical depth (Eq. 18) is given by

$$\tau_{\min} = \begin{cases} \frac{\mathcal{L}}{\mathcal{E}^{\beta_p+1}} \delta_D^{2(\beta_p-1)} & ; \text{PL \& limit A,} \\ \frac{\mathcal{L}}{\mathcal{E}^{\beta_p+1}} \delta_D^{\beta_p-3} & ; \text{PL \& limit B,} \\ \frac{\mathcal{L}}{\mathcal{E}^{\alpha_p}} \delta_D^{2(\alpha_p-2)} \exp\left(-\frac{\delta_D^2}{\mathcal{E}}\right) & ; \text{CPL \& limit A,} \\ \frac{\mathcal{L}}{\mathcal{E}^{\alpha_p}} \delta_D^{\alpha_p-4} \exp\left(-\frac{\delta_D}{\mathcal{E}}\right) & ; \text{CPL \& limit B,} \\ \frac{\mathcal{L}\mathcal{E}}{\Gamma \delta_D^5} & ; \text{limit C.} \end{cases} \quad (23)$$

These equations can be rewritten as limits on the Doppler factor in term of the observed parameters for limits A and B. In particular, for PL spectrum, we obtain by setting $\tau_{\gamma, \min} = 1$:

$$\delta_{D, \min} = \begin{cases} (\mathcal{E}^{\beta_p+1}/\mathcal{L})^{\frac{1}{2(\beta_p-1)}} & ; \text{PL \& limit A,} \\ (\mathcal{E}^{\beta_p+1}/\mathcal{L})^{\frac{1}{\beta_p-3}} & ; \text{PL \& limit B.} \end{cases} \quad (24)$$

Once the Doppler factor, $\delta_{D, \min}$, is known, we have:

$$\theta(\Gamma) = \arccos \left[\frac{\Gamma \delta_{D, \min} - 1}{\delta_{D, \min}(\Gamma^2 - 1)^{1/2}} \right]; \text{ limits A \& B.} \quad (25)$$

The minimal Lorentz factor is obtained by setting $\theta = 0$ as

$$\Gamma_{\min} = \frac{\delta_{D, \min}^2 + 1}{2\delta_{D, \min}} \quad \left[\approx \delta_{D, \min}/2 \right]. \quad (26)$$

The maximal angle for a given $\delta_{D, \min}$ is

$$\theta_{\max} = \arcsin(\delta_{D, \min}^{-1}) \quad \left[\approx 1/2\Gamma_{\min} \right], \quad (27)$$

and the Lorentz factor at the maximal angle is

$$\Gamma(\theta_{\max}) = 1/\sin \theta_{\max} \quad \left[\approx 2\Gamma_{\min} \right]. \quad (28)$$

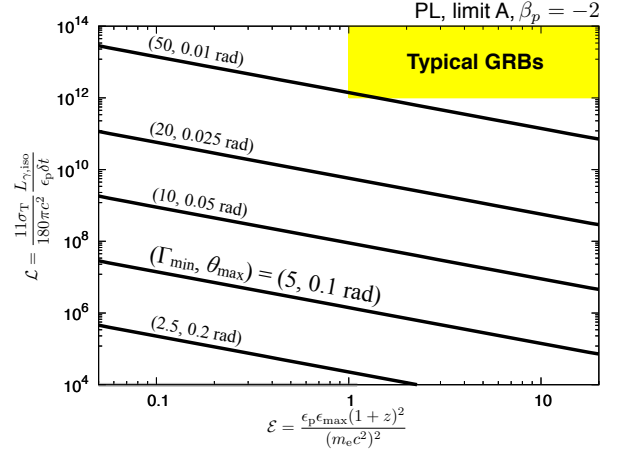


Figure 3. Contours lines of the maximal viewing angle, θ_{\max} , and the minimal Lorentz factor, Γ_{\min} , for a PL spectrum and limit A (the spectral index is fixed $\beta_p = -2$). The yellow shaded region show the parameter space of normal GRBs with $\mathcal{L} \gtrsim 10^{12}$ and demonstrates that typical GRBs are unlikely to be observed from an off-axis view.

Where the approximate values in the square brackets are valid for $\delta_{D, \min} \gg 1$.

For limit C, since an additional factor of Γ appears in Eq. (23), we approximately derive the allowed region for on-axis and off-axis regions separately. In the on-axis regime, using Eq. (20) one obtains $\tau_{\min} = 1$ for:

$$\Gamma = \Gamma_{\min} \simeq \left(\frac{\mathcal{L}\mathcal{E}}{32} \right)^{1/6}; \text{ limit C.} \quad (29)$$

In the off-axis regime, $\tau_{\min} = 1$ is obtained for an angle

$$\theta(\Gamma) \simeq \left(\frac{\mathcal{L}\mathcal{E}}{32} \right)^{-1/10} \Gamma^{-2/5}, \quad (30)$$

which is a decreasing function of Γ . Since in this regime $\theta > 1/\Gamma$ the maximal angle may be reasonably evaluated by Eq. (27), $\theta_{\max} \simeq 1/2\Gamma_{\min}$, as for limits A and B.

Tables 1 and 2 summarize the results of this paper. In Table 2, we list the definitions of the parameters \mathcal{L} and \mathcal{E} , that are obtained by the observables in Table 1, and the expressions for the optical depth and the resulting limits on δ_D , Γ , and θ (if it is analytically derived) for each spectrum.

Fig. 3, depicts the contours of a fixed θ_{\max} and Γ_{\min} as a function of the observables \mathcal{L} and \mathcal{E} for a PL spectrum in limit A, which is relevant for typical GRBs. Due to the power-law dependence of τ_{\min} on \mathcal{L} and \mathcal{E} , the contours are straight lines. A small \mathcal{E} implies a large energy threshold for pair creation, which reduces the photon fraction and hence the compactness limits are relaxed leading to a lower values of Γ_{\min} and larger values of θ_{\max} . The yellow shaded region in this figure corresponds to typical GRBs with $\mathcal{L} \gtrsim 10^{12}$. These GRBs have very small maximal viewing angles $\theta_{\max} \lesssim 10^{-2}$ rad. The chance to observe such a GRB off-axis (relative to observing it on-axis) is $\theta_{\max}/\theta_j \ll 1$ where θ_j is the jet opening angle of the GRB. In other words, it is hardly possible that regular GRBs are viewed off-axis (see also §3.1).

Fig. 4 depicts contour lines of Γ_{\min} and θ_{\max} for a CPL

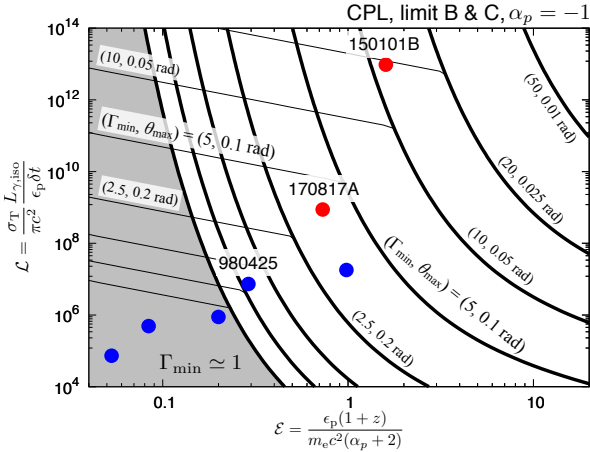


Figure 4. The same as Fig. 3 but for a CPL spectrum and limits B and C with $\alpha_p = -1$. The thick curves denote the contours of limit B for fixed values of $\theta_{\max} = 0.01, 0.025, 0.05$, and 0.1 to 0.5 rad with 0.1 rad steps and the corresponding Γ_{\min} values. The contours for limit C are also shown with thin curves in the region where limit C is more constraining than limit B. The values of Γ_{\min} and θ_{\max} of these contours are the same as those on the B contours in which they end. The red and blue points show observed sGRB and uGRBs, respectively. The grey shaded region denotes a parameter region where a relativistic motion is not required.

spectrum in limits B ($\alpha_p = -1$) and C. These limits are relevant for low luminosity γ -ray transients (see §3). Since the CPL spectrum is exponential, the contours have no longer a simple form. The contour's shape does not change much for a different value of α_p because the spectral index is absorbed into the definition of \mathcal{E} and it disappears from the exponential. Also shown are Γ_{\min} and θ_{\max} dictated by limit C. This limit becomes important for low luminosity bursts (e.g., left panel of Fig. 2). The contours for limit C are given by

$$\mathcal{L} \sim \frac{m_p \theta_{\max}^{-6}}{2m_e(\alpha_p + 2)\mathcal{E}} \simeq 9.2 \times 10^8 \left(\frac{\theta_{\max}}{0.1 \text{ rad}} \right)^{-6} \frac{1}{(\alpha_p + 2)\mathcal{E}}. \quad (31)$$

Note that in this equation, the parameter \mathcal{E} is defined for limit B (see Eq. 22) and overall the limit is independent of the spectral shape, as expected. Like in limit A, a smaller \mathcal{E} values allow larger viewing angles. However, if \mathcal{E} is too small, limit C constrains the maximal angle more strictly. We also find that for events with $\mathcal{L} \lesssim 10^{7-8}$ and $\mathcal{E} \lesssim 0.1$, the compactness considerations do not require a relativistic motion of the γ -ray sources.

3 APPLICATION TO γ -RAY TRANSIENTS

We turn now to apply the generalized compactness argument to specific events (listed up in Table 3) focusing on those events that have been discussed in the context of off-axis emission models.

3.1 Typical GRBs

We begin with a discussion of the compactness constraint on ordinary bright GRBs. These bursts have a large γ -ray

luminosity $L_{\gamma, \text{iso}} \gtrsim 10^{51} \text{ erg s}^{-1}$ and a rapid time variability $\delta t \sim 0.01 - 0.1$ s. These give rise to a large $\mathcal{L} \gtrsim 10^{12}$ (Since we consider limit A we add an additional factor $11/180$ to Eq. 19). The allowed parameter region for typical GRBs is shown in Fig. 3 and the specific limits on GRB 090510 (Ackermann et al. 2010) are shown on the right panel of Fig. 2. Note that GRB 090510 is one of the brightest and hardest GRBs and hence its limits are tighter than those of a typical GRB. The large value of \mathcal{L} in typical GRBs implies that Γ_{\min} and θ_{\max} are tightly limited as $\Gamma_{\min} \gtrsim 10^2$ and $\theta_{\max} \lesssim 10^{-2}$ rad. The very small allowed viewing angle justifies the commonly adopted “on-axis” assumption and limits the chance that a typical GRB is viewed by an off-axis observers.

For typical GRBs the commonly used limit A is the dominant one. Limit B is applicable for softer bursts and in particular for weak bursts with a CPL spectrum. Limit C is hardly important for typical bursts, but it is used, implicitly, in regular GRBs in the context of photospheric emission models.

3.2 GRB170817A

Next, we revisit the compactness of GRB 170817A (Kasliwal et al. 2017; Gottlieb et al. 2018; Matsumoto et al. 2019). The very dim γ -ray luminosity motivated some authors to consider an off-axis emission model, where the γ -ray emission is produced from a relativistic jet core. However, the constraint on the angular configuration from the compactness showed that the γ -ray emitting region should be closer to our line of sight than the jet core (Matsumoto et al. 2019, see also Ioka & Nakamura 2019).

Fig. 5 depicts the allowed $(\Gamma, \theta_{\text{obs}})$ region derived by imposing $\tau_{\min} < 1$. Since both limits B and C can be important for dim bursts (see below), we show the allowed region for both limits (red and magenta curves). There is a maximal allowed viewing angle as we discussed in §2.3. The Lorentz factor and viewing angle are constrained to be $\Gamma_{\min} = 3.7(4.2)$ and $\theta_{\max} = 0.13(0.17)$ rad by limits (C), respectively. We stress again that for limit B we assume that the exponential photon spectrum extends to higher energies than the observed ones.³ But there is no reason to expect a super-exponential spectrum at higher energies. On the other hand limit C is independent of the spectrum. We also remark that the maximal angle given by limit B, θ_{\max} is smaller by about a factor of 2 than that obtained by Matsumoto et al. (2019) (see their Fig. 2). This is because of a different definition of the angle. Here θ is the measured from the center of the γ -ray emitting region while in Matsumoto et al. (2019) it is the angular distance from the edge of the γ -ray emitting region. Moreover, Matsumoto et al. (2019) have approximated the Doppler factor $\delta_D(\theta, \Gamma) \sim 2/(\Gamma\theta^2)$, and this approximation breaks down for low Lorentz factor.

3.3 GRB 150101B

GRB 150101B is one of the nearest sGRBs (Troja et al. 2018; Burns et al. 2018). Its γ -ray isotropic equivalent energy

³ §4 of Matsumoto et al. (2019) discusses a spectrum independent limit that pair production opacity imposes on the source of emission in GW170817.

Table 3. Observables and the derived Γ_{\min} of selected γ -ray transients. The most constraining limit is denoted by boldface. For GRB 170817A and 150101B, the first and second lines show the observables given by time-resolved spectral analysis and ones by time-integrated analysis. * Note that the analysis breaks down for Γ_{\min} values approaching unity.

Event (Ref)	Observables							Limit : $\Gamma_{\min}(\sim 1/2\theta_{\max})$		
	$L_{\gamma, \text{iso}}$ [erg s $^{-1}$]	δt [s]	ϵ_p [keV]	ϵ_{\max} [keV]	β_p (PL)	α_p (CPL)	z	limit A	limit B	limit C
GRB 090510 (1)	10^{53}	0.01	4000	3×10^7	-	-	0.9	910	690	66
GRB 170817A (2,3,4)	2×10^{47}	0.2	520	520	-	-0.6	0.008	1.7	3.7	4.2
			185	-	-	-	-	1.3	2.0	4.2
GRB 150101B (5)	10^{51}	0.01	1300	1300	-	-0.8	0.1	5.5	17	29
			550	-	-	-	-	3.6	7.9	21
GRB 980425 (6,7,8)	6×10^{46}	10	70	200	-2.3	-	0.009	2.2	3.7	1.9*
			120	-	-	-1.2	-	1*	1.5*	1.9*
GRB 031203 (9)	10^{48}	40	> 200	400	-	-1.6	0.1	1.5*	3.2	2.3
GRB 060218 (8,10)	3×10^{46}	2000	30	100	-	-0.9	0.03	1*	1*	1*
GRB 100316D (11)	3×10^{46}	300	30	-	-	-1.4	0.06	-	1*	1.2*
GRB 171205A (12)	10^{47}	140	120	1000	-	-0.85	0.04	1.2*	1.2*	1.4*

Refs. (1) Ackermann et al. (2010), (2) Goldstein et al. (2017), (3) Veres et al. (2018), (4) Abbott et al. (2017a), (5) Burns et al. (2018), (6) Galama et al. (1998), (7) Frontera et al. (2000), (8) Kaneko et al. (2007), (9) Sazonov et al. (2004), (10) Campana et al. (2006), (11) Starling et al. (2011), (12) D’Elia et al. (2018)

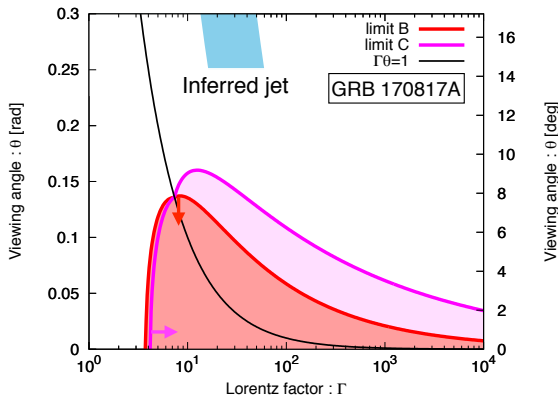


Figure 5. The allowed region of the Lorentz factor and the viewing angle determined by the compactness argument for GRB 170817A for limits B (red) and C (magenta). The parameters are set by $L_{\gamma, \text{iso}} = 2 \times 10^{47} \text{ erg s}^{-1}$, $\delta t = 0.2 \text{ s}$, $\epsilon_p = 520 \text{ keV}$, and $\alpha_p = -0.6$ (see Table 3). The blue shaded region depicts the required parameters for the emission to arise from the jet that was inferred from the afterglow observations.

$E_{\gamma, \text{iso}} \sim 10^{49} \text{ erg}$ is relatively small. It has a CPL spectrum with a rather large peak photon energy, $\epsilon_p \sim 1300 \text{ keV}$, and it is highly variable, $\delta t \sim 0.01 \text{ s}$ (see Table 3). GRB 150101B also shows a bright optical and long-time X-ray afterglows. Troja et al. (2018) suggested that we have observed an off-axis emission with angular distance of $\theta \sim 10 \text{ deg} \simeq 0.18 \text{ rad}$, the strong optical afterglow is a macronova signal and the long-time X-ray emission is the off-axis afterglow. Since GRB 150101B is not as dim as GRB 170817A, compactness gives a tighter constraint on the maximal angle. We find that $\theta_{\max} \lesssim 0.05 \text{ rad}$ (see Fig. 4). This constraint rules out the off-axis model, which requires a much larger viewing angle. The minimal Lorentz factor is constrained to be $\Gamma_{\min} \simeq 20$.

Several authors suggested that the origin of the γ -rays in GW170817 is the shock breakout of the cocoon (Kasliwal

et al. 2017; Nakar et al. 2018; Gottlieb et al. 2018; Bromberg et al. 2018; Pozanenko et al. 2018; Beloborodov et al. 2018). Interestingly, the observed γ -rays from GRB 150101B satisfies the closure relation for relativistic shock breakouts (Nakar & Sari 2012). A breakout radius of $R \sim 10^{12} \text{ cm}$ and a Lorentz factor of $\Gamma \sim 35$ are predicted to produce a $\delta t \sim 0.01 \text{ s}$ pulse with $\epsilon_p \sim 1300 \text{ keV}$ and a total energy of $E_{\gamma, \text{iso}} \sim 10^{49} \text{ erg}$. The breakout radius is similar to the one suggested for GW170817 (Nakar et al. 2018). The higher Lorentz factor is expected if the breakout is driven by a cocoon and is observed at an angle that is closer to the jet axis than in GW170817, as implied by the afterglow of GRB 150101B. This supports a picture where both GRBs 170817A and 150101B are generated by shock breakouts, where the main difference is the angle with respect to the jet axis and thus the Lorentz factor of the shock.

3.4 Low luminosity GRBs (*ll*GRBs)

*ll*GRBs are a subclass of long GRBs (*l*GRBs) whose properties are very different from those of typical *l*GRBs, such as much lower luminosity $\sim 10^{46-48} \text{ erg s}^{-1}$, lower peak photon energy $\lesssim 100 \text{ keV}$, a smooth light curve and a longer entire duration $\gtrsim 100 \text{ s}$ (Kulkarni et al. 1998; Campana et al. 2006; Soderberg et al. 2006; Kaneko et al. 2007; Bromberg et al. 2011). Table 3 describes the observables of several *ll*GRBs. In particular, the lower photon energy and lesser time variability suggest weak relativistic boosts. However, both *l*GRBs and *ll*GRBs are associated with peculiar broad-line type Ic SNe, which suggests that they share the same progenitors (e.g., Nakar 2015). A common hypothesis that *ll*GRBs are ordinary GRBs viewed off-axis (Nakamura 1998; Eichler & Levinson 1999; Woosley et al. 1999; Ioka & Nakamura 2001; Yamazaki et al. 2003; Waxman 2004) is problematic because their afterglow observations do not show the expected off-axis afterglow signature (e.g., Soderberg et al. 2006, for GRB 060218).

Fig. 6 shows the compactness limits B and C for *ll*GRB 980425. As both PL and CPL spectra were fitted to this event (see Table 3) we use both types of spectra. The PL

limits are quite constraining, but the CPL limits as well as limit C that is independent of the spectrum show that a rather large region in the phase space is allowed with an observing angle of up to ~ 0.4 rad.

Assuming that this burst was produced by an ordinary GRB with $E_{\gamma, \text{iso, obs}}(\theta = 0) \sim 10^{50-52}$ erg but viewed from off-axis (see e.g., Ioka & Nakamura 2001; Yamazaki et al. 2003) we estimate the allowed parameter region for the off-axis model (shown as a blue shaded band in Fig. 6). Indeed there is an overlap between the two regions, thus strictly speaking compactness cannot rule out the off-axis model. However the required region is constrained with a maximal viewing angle $\theta_{\text{max}} \sim 0.2 - 0.3$ rad. The constraint is more severe if we assume that the on-axis emission of *GRB 980425* was a regular GRB with a typical Lorentz factor $\Gamma \gtrsim 10^2$. This would constrain the observing angle to be $\lesssim 0.06$ rad, making the off-axis scenario extremely unlikely and already ruled out by radio afterglow observations (Soderberg et al. 2004).

Like in GRB 980425 (see Fig. 6), for other *GRBs*, compactness cannot exclude the off-axis scenario. However, the compactness argument is still useful to constrain the allowed parameter region and becomes more powerful by combining afterglow observations. As shown in Fig. 4, most *GRBs* have larger maximal angle than that of GRB 980425 because of their small peak energy ϵ_p . In particular, compactness does not necessarily require a relativistic outflow for GRBs 060218 and 100316D.

If we require ordinary IGRBs with $\Gamma \gtrsim 10^2$ to produce the *GRBs*, the constraint on the viewing angle becomes more severe as shown for GRB 980425 in Fig. 6. The maximal off-axis viewing angles for *GRBs* 031203, 060218, 100326, and 171205, (assuming from regular IGRB sources with $\Gamma \gtrsim 10^2$) are $\theta_{\text{max}} = 0.064, 0.28, 0.17$, and 0.11 rad, respectively. For GRB 031203, Ramirez-Ruiz et al. (2005) gave $\theta_{\text{obs}} \sim 2\theta_j \sim 0.14$ rad. This is marginally excluded by compactness. For GRB 060218, Soderberg et al. (2006) excluded the viewing angles $\theta \lesssim 1.1$ rad. Combining the compactness constraints, we can exclude the off-axis model for this event.

While as stated above the compactness limit on its own cannot rule out the possibility that *GRBs* are regular IGRBs viewed off-axis, its implication are still far reaching. In particular, the very small viewing angle implied by this argument (see Figs. 6 and 4) and in particular the smaller angles implied with assuming typical IGRB sources with $\Gamma \gtrsim 10^2$ suggest that the rate of off-axis viewed IGRBs should be rather small as compared with the rate of regular IGRBs. On the other hand the observations imply that, while there are only few observed *GRBs*, their intrinsic rate is about ten times larger than the rate of IGRBs (see e.g. Soderberg et al. 2006).

4 SUMMARY

We extended here the compactness formalism, that was commonly used for on axis observers, to an observer at a general viewing angle. We derived an expression for the optical depth of the γ -ray emitting region for three limits on the opacity (see Lithwick & Sari 2001): Limit A is the commonly used one and it imposed that the highest energy photon can

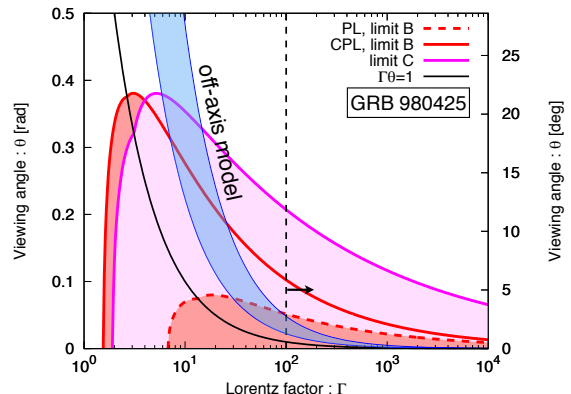


Figure 6. The allowed region of the Lorentz factor and the viewing angle for *GRB 980425*. The parameters are set by $L_{\gamma, \text{iso}} = 6 \times 10^{46}$ erg s $^{-1}$, $\delta t = 10$ s, $\epsilon_p = 70$ keV and $\beta_p = -2.3$ (for PL spectrum), and 120 keV and $\alpha_p = -1.2$ (for CPL spectrum) (see Table 3). In the off-axis model, the Lorentz factor and viewing angle are constrained within the blue shaded region. The thin dashed vertical line marks the typical minimal Lorentz factor for regular GRBs. Thus if *GRB 980425* was a regular IGRB viewed off-axis it should have been to the right of this line, allowing for a very small viewing angles, a possibility that is ruled out by radio afterglow observations (Soderberg et al. 2004).

escape from the source. The other limits are less known (see however Lithwick & Sari 2001). Limit B requires that the number of pairs produced is sufficiently small so that the system remains optically thin to Compton scattering. In limit C, which is valid only for baryonic outflow, the electron accompanying the baryons should be optically thin for γ -rays. We also considered two common spectral shapes (a single power-law and a power-law with an exponential cut-off), and the analysis can be easily extended to other spectral shapes. By imposing that the optical depth is smaller than unity, we obtain the allowed condition on the Lorentz factor Γ and viewing angle θ . A given event can be characterized by two dimensionless parameters \mathcal{E} and \mathcal{L} (see Eqs. 19 and 22), and the spectral index (α_p or β_p). The resulting limits are summarized in Tables 1 and 2.

We find that the minimal Lorentz factor is obtained for an on-axis observer, $\theta = 0$, this configuration is the same as the one discussed in previous works (e.g., Lithwick & Sari 2001). Interestingly, we find that there is a maximal allowed viewing angle θ_{max} for each event. This maximal viewing angle satisfies $\Gamma \theta_{\text{max}} \approx 1$, thus it is on the boundary between being on-axis and off-axis.

We applied the generalized compactness argument to the weak sGRBs 170817A and 150101B, and to several *GRBs*. For GRB 170817A, we confirmed earlier results (Kasliwal et al. 2017; Lazzati et al. 2018; Kathirgamaraju et al. 2018; Gottlieb et al. 2018; Bromberg et al. 2018; Pozanenko et al. 2018; Matsumoto et al. 2019) that the observed relativistic jet core could not be the origin of the γ -rays in GRB 170817A. For the weak sGRB 150101B that was proposed to be an off-axis sGRB (Troja et al. 2018; Burns et al. 2018) we find a severe limit on the viewing angle, strongly disfavoring the off-axis option. For *GRBs*, we find that the off-axis emission scenario cannot be excluded by com-

compactness argument alone. However, compactness arguments limit strongly the allowed parameter phase space for such models, which when combined with other constraints, make an off-axis origin highly unlikely. Finally we find that regular GRBs (both long and short) can be viewed off axis only from a very small viewing angles. Thus the chance that we have observed a regular GRB off-axis is slim.

ACKNOWLEDGMENTS

This research is supported by the CHE-ISF I-Core center for excellence in Astrophysics. TM is supported by JSPS Overseas Challenge Program for Young Researchers and by Grant-in-Aid for JSPS Research Fellow 17J09895. TP is supported by an advanced ERC grant TReX and by the Templeton foundation. EN is partially supported by an consolidator ERC grant (JetNS) and an ISF grant.

APPENDIX A: THE LIGHT CROSSING TIME

First we show that if $\delta t_{lc} > (\delta t_{radial}, \delta t_{ang})$, i.e. the light crossing time is the longest, then the limits on the opacity are more constraining or equal to those obtained otherwise. Namely, that the least constraining limit on τ is obtained when $l' \simeq \Delta R'$. We will show that for the two limits of fully on-axis observer, $\theta = 0$, and fully off axis observer, $\theta \gg 1/\Gamma$. Consider a photon released at a radius R towards the observer from a point source that moves radially at a Lorentz factor Γ . By the time that the photon have reached $2R$ the point source have reached a radius $R(1 + \beta/\cos\theta)$, so the radial distance between the source and the photon is at this time is $d = R(1 - \beta/\cos\theta)$, which for $\theta = 0$ is $d \simeq R/2\Gamma^2$ and for $1/\Gamma \ll \theta \ll 1$ it is $d \simeq R\theta^2/2$. Now, $l \simeq \min\{d, \Delta R\}$ and let's define $q > 1$ such that $\Delta R = qd$, and $\delta t_{lc} = qd/c$. This is compared to the radial time that for $dR = R$ is $\delta t_{radial} = d/c$ (both on- and off-axis). Finally, $l'/\Delta R' = l/\Delta R = \min\{1, 1/q\}$. With all these we can now compare τ between the case that the light crossing time dominates, i.e., $q > 1$ and the case that the radial time dominates. From Eq. (6) we see that for $q < 1$ the optical depth is independent of q . But, when $q > 1$ the optical depth must be smaller by at least a factor of q . The reason is that when $q > 1$ the limit $\delta t_{radial} < \delta t_{lc}$ implies that R is smaller than ΔR by at least a factor of q . This implies that the least constraining limit on τ is obtained for $q < 1$, namely the width of the emitting region is small enough so that the light crossing time can be neglected.

APPENDIX B: ANGULAR TIMESCALE VS. RADIAL TIMESCALE CONSTRAINS

We show first that in the off-axis case the limit on τ obtained under the assumption that $\delta t = \delta t_{ang}$, is similar to the one obtained in case that $\delta t = \delta t_{rad}$ and $dR = R$. In off-axis case with $1/\Gamma \ll \theta \ll 1$, the angular time and radial time are approximately

$$\delta t_{ang} = \frac{2R}{c} \sin(\theta) \sin\left(\frac{\theta_\gamma}{2}\right) \simeq \frac{R\theta\theta_\gamma}{c}, \quad (B1)$$

and

$$\delta t_{radial} \simeq \frac{dR\theta^2}{c}, \quad (B2)$$

respectively. Note that for brevity, we ignore here numerical factors of order unity. We focus on the factor $1/(\theta_\gamma R)^2$ in the optical depth (Eq. 17). All other factors are identical for both cases. When $\delta t = \delta t_{ang}$, this factor becomes $1/(\theta_\gamma R)^2 \simeq (\theta/c\delta t)^2$. On the other hand, when $\delta t = \delta t_{radial}$ with $dR = R$, we obtain the same expression:

$$\frac{1}{(\theta_\gamma R)^2} \simeq \left(\frac{\theta^2}{\theta_\gamma c\delta t}\right)^2 = \left(\frac{\theta}{c\delta t}\right)^2, \quad (B3)$$

where we used $\theta_\gamma = \max(\theta, 1/\Gamma) = \theta$, as the larger value of θ_γ minimizes τ .

The limit on τ becomes similar in both cases for an on-axis observer ($\theta \ll 1/\Gamma$), unless there is an anomalously narrow source with $\theta_\gamma \ll 1/\Gamma$. The timescales are given by

$$\delta t_{ang} = \frac{2R}{c} \left\{ 1 - \cos\left[\frac{1}{2}\left(\theta + \frac{\theta_\gamma}{2}\right)\right] \right\} \simeq \frac{R\theta_\gamma^2}{c}, \quad (B4)$$

and

$$\delta t_{radial} \simeq \frac{dR}{c\Gamma^2}. \quad (B5)$$

While the assumption of $\delta t = \delta t_{ang}$ gives the factor

$$\frac{1}{(\theta_\gamma R)^2} \simeq \left(\frac{\theta_\gamma}{c\delta t}\right)^2, \quad (B6)$$

the case $\delta t = \delta t_{radial}$ with $dR = R$ gives

$$\frac{1}{(R\theta_\gamma)^2} \simeq \left(\frac{1}{\theta_\gamma \Gamma^2 c\delta t}\right)^2. \quad (B7)$$

The factor $1/(\theta_\gamma R)^2$ becomes the same expression for both cases for an emitting region with a reasonable angular extent $\theta_\gamma \sim 1/\Gamma$.

REFERENCES

- Abbott B. P., et al., 2017a, [Physical Review Letters](#), **119**, 161101
- Abbott B. P., et al., 2017b, [ApJ](#), **848**, L13
- Ackermann M., et al., 2010, [ApJ](#), **716**, 1178
- Band D., et al., 1993, [ApJ](#), **413**, 281
- Beloborodov A. M., Lundman C., Levin Y., 2018, arXiv e-prints, [p. arXiv:1812.11247](#)
- Bromberg O., Nakar E., Piran T., 2011, [ApJ](#), **739**, L55
- Bromberg O., Tchekhovskoy A., Gottlieb O., Nakar E., Piran T., 2018, [MNRAS](#), **475**, 2971
- Burns E., et al., 2018, [ApJ](#), **863**, L34
- Campana S., et al., 2006, [Nature](#), **442**, 1008
- D'Elia V., et al., 2018, [A&A](#), **619**, A66
- Eichler D., 2017, [ApJ](#), **851**, L32
- Eichler D., Levinson A., 1999, [ApJ](#), **521**, L117
- Frontera F., et al., 2000, [ApJS](#), **127**, 59
- Galama T. J., et al., 1998, [Nature](#), **395**, 670
- Goldstein A., et al., 2017, [ApJ](#), **848**, L14
- Goodman J., 1986, [ApJ](#), **308**, L47
- Gottlieb O., Nakar E., Piran T., Hotokezaka K., 2018, [MNRAS](#), **479**, 588
- Ioka K., Nakamura T., 2001, [ApJ](#), **554**, L163
- Ioka K., Nakamura T., 2018, [Progress of Theoretical and Experimental Physics](#), **2018**, 043E02
- Ioka K., Nakamura T., 2019, arXiv e-prints,

- Kaneko Y., et al., 2007, *ApJ*, **654**, 385
- Kasliwal M. M., et al., 2017, *Science*, **358**, 1559
- Kathirgamaraju A., Barniol Duran R., Giannios D., 2018, *MNRAS*, **473**, L121
- Krolik J. H., Pier E. A., 1991, *ApJ*, **373**, 277
- Kulkarni S. R., et al., 1998, *Nature*, **395**, 663
- Lazzati D., Perna R., Morsony B. J., Lopez-Camara D., Cantiello M., Ciolfi R., Giacomazzo B., Workman J. C., 2018, *Physical Review Letters*, **120**, 241103
- Lithwick Y., Sari R., 2001, *ApJ*, **555**, 540
- Matsumoto T., Nakar E., Piran T., 2019, *MNRAS*, **483**, 1247
- Mooley K. P., et al., 2018, *Nature*, **561**, 355
- Murguia-Berthier A., et al., 2017, *ApJ*, **848**, L34
- Nakamura T., 1998, *Progress of Theoretical Physics*, **100**, 921
- Nakar E., 2007, *Phys. Rep.*, **442**, 166
- Nakar E., 2015, *ApJ*, **807**, 172
- Nakar E., Sari R., 2012, *ApJ*, **747**, 88
- Nakar E., Gottlieb O., Piran T., Kasliwal M. M., Hallinan G., 2018, *ApJ*, **867**, 18
- Paczynski B., 1986, *ApJ*, **308**, L43
- Piran T., 1997, in Bahcall J. N., Ostriker J. P., eds, *Unsolved Problems in Astrophysics*. pp 343–377
- Piran T., 1999, *Phys. Rep.*, **314**, 575
- Pozanenko A. S., et al., 2018, *ApJ*, **852**, L30
- Ramirez-Ruiz E., Granot J., Kouveliotou C., Woosley S. E., Patel S. K., Mazzali P. A., 2005, *ApJ*, **625**, L91
- Ruderman M., 1975, in Bergman P. G., Fenyves E. J., Motz L., eds, *Annals of the New York Academy of Sciences Vol. 262, Seventh Texas Symposium on Relativistic Astrophysics*. pp 164–180, doi:10.1111/j.1749-6632.1975.tb31430.x
- Savchenko V., et al., 2017, *ApJ*, **848**, L15
- Sazonov S. Y., Lutovinov A. A., Sunyaev R. A., 2004, *Nature*, **430**, 646
- Schmidt W. K. H., 1978, *Nature*, **271**, 525
- Soderberg A. M., Frail D. A., Wieringa M. H., 2004, *ApJ*, **607**, L13
- Soderberg A. M., et al., 2006, *Nature*, **442**, 1014
- Starling R. L. C., et al., 2011, *MNRAS*, **411**, 2792
- Svensson R., 1987, *MNRAS*, **227**, 403
- Troja E., et al., 2018, *Nature Communications*, **9**, 4089
- Veres P., et al., 2018, preprint, ([arXiv:1802.07328](https://arxiv.org/abs/1802.07328))
- Waxman E., 2004, *ApJ*, **602**, 886
- Woltjer L., 1966, *ApJ*, **146**, 597
- Woosley S. E., Eastman R. G., Schmidt B. P., 1999, *ApJ*, **516**, 788
- Yamazaki R., Yonetoku D., Nakamura T., 2003, *ApJ*, **594**, L79

This paper has been typeset from a \LaTeX file prepared by the author.